Fuel 217 (2018) 297–305

Contents lists available at ScienceDirect

Fuel

journal homepage: www.elsevier.com/locate/fuel

Full Length Article

Cu-BTC as a novel material for elemental mercury removal from sintering gas

Dongyao Chen[a], Songjian Zhao[a,b,*], Zan Qu[a,*], Naiqiang Yan[a]

[a] School of Environmental Science and Engineering, Shanghai Jiao Tong University, 800 Dong Chuan Road, Shanghai 200240, PR China
[b] School of Chemistry and Chemical Engineering, Shanghai Jiao Tong University, 800 Dong Chuan Road, Shanghai 200240, PR China

GRAPHICAL ABSTRACT

The reaction process for the Hg^0 removal over Cu-BTC.

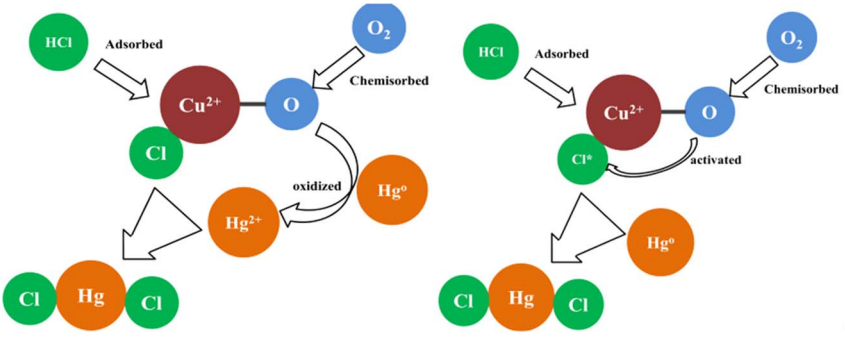

ARTICLE INFO

Keywords:
Cu-BTC
MOFs
Mercury removal
Sintering gas

ABSTRACT

Cu-BTC, as one of the metal organic frameworks (MOFs), was prepared and employed for the capture of elemental mercury (Hg^0) in sintering gas. The material was characterized using TGA, XPS, XRD, BET surface measurement and TEM. Results showed that Cu-BTC had good microscopic morphologies, large BET surface area and high thermal stability, which make it suitable for sintering gas. The Hg^0 removal performance was investigated under different conditions. Cu-BTC had limited Hg^0 removal ability without HCl, but exhibited an excellent Hg^0 removal efficiency when 15 ppm HCl was added. HCl and O_2 played an important role for the Hg^0 removal efficiency when they were at low concentration. According to the results of Hg^0 removal performance and physiochemical characterization, the mechanism of Hg^0 capture was speculated with and without HCl. Furthermore, the influence of SO_2, NO and H_2O were studied. SO_2 has inhibition effect on the removal of Hg^0, while NO can promote the Hg^0 removal. As for H_2O, it has nearly no effect on mercury removal. When HCl and O_2 were at high concentration, the influence of SO_2, NO and H_2O are not significant.

1. Introduction

Mercury is regarded as one of the most life-threatening pollutants because of its high volatilization, stable chemical properties and the easy accumulation in living things [1]. Mercury in gas phase exists mainly in the form of elemental mercury (Hg^0), which has a long lifetime allowing for global dispersion [2,3]. The gas phase mercury can also transfer to the water and soild by deposition, and the inorganic form of mercury can be converted into methylmercury by some bacteria (e.g., iron reducing bacteria and sulfate reducing bacteria) [1,4]. Then

* Corresponding authors at: School of Environmental Science and Engineering, Shanghai Jiao Tong University, 800 Dong Chuan Road, Shanghai 200240, PR China.
E-mail addresses: zhaosongjian@sjtu.edu.cn (S. Zhao), quzan@sjtu.edu.cn (Z. Qu).

https://doi.org/10.1016/j.fuel.2017.12.086
Received 7 August 2017; Received in revised form 15 December 2017; Accepted 20 December 2017

the methylmercury bioaccumulates through the food chain, and affect wildlife, domestic animals, and humans alike [5]. The consumption of marine and freshwater foods is the majority of human methylmercury exposure [6].The famous Minamata disease in Japan is a classic example of the health hazards of mercury.

As one of the important anthropogenic sources of atmospheric mercury, iron and steel production contributed about 46 t of the total atmospheric mercury emissions in 2010 [7]. China made 822.7 million tons of crude steel in 2014 [8], and since the mercury emission characteristics is about 0.04 g Hg/ton steel [7,9,10], the mercury emission from iron and steel production in China can be calculated to be 32.9 t. Although this emission is less than the emissions from coal combustion (292 t [11]), nonferrous metal smelting (97.4 t [12]) and cement production (75.1 t [13]), it still cannot be ignored. And the sintering process can provide more than half of the mercury emissions from iron and steel production [14]. Now, it can be seen that sintering process has been an important mercury source. Therefore, mercury removal from sintering gas is the key for the control of mercury emission from iron and steel production.

Currently, mercury is removed mainly by desulfurization devices, selective catalytic reduction (SCR) process and activated carbon. Oxidized mercury (Hg^{2+}) can be absorbed by desulfurization devices and activated carbon. However, since a substantial portion of mercury exists in the form of elemental mercury (Hg^0), desulfurization devices and activated carbon have limited removal rate because of its high volatility and low solubility in water [15]. Hg^0 can be oxidized to Hg^{2+} with the help of SCR catalyst, and then be removed by desulfurization devices [16], but the catalytic efficiency was limited by the temperature windows. The optimal temperature of conventional SCR is 350–450 °C, while the temperature of the sintering gas is in the range of 120–180 °C [17], and the conventional SCR catalysts may be inactive at this low temperature [18]. Recently solid supported ionic liquids have shown remarkable Hg^0 removal capacity from natural gas at lab and industrial scale [19,20], however, high temperature of sintering gas as compared to natural gas, restricts their application for Hg^0 removal from sintering gas as well.

Thus, materials with higher mercury removal efficiency for sintering gas are needed.

Metal organic frameworks (MOFs), consisting of metal center and organic ligands, have emerged as the novel porous crystalline materials due to their high surface areas, tunable pore sizes, high thermal stability, and tailorable chemistry [21,22]. They have recently attracted widespread research interests in gas storage and separation [23–25], drug delivery [26], and heterogeneous catalysis [27–29].

Cu-BTC (BTC = benzene-1,3,5-tricarboxylate) is a well known copper-based MOF with a 3D square-shaped channel system [30]. It was first reported by Williams et al. [31]. At present, most of the researches of Cu-BTC mainly focus on gas capture and chemical production [32–34]. Since Cu-BTC exhibited favorable catalytic and adsorptive performance in the previous research, it might have the potential to be used for mercury removal, but there are not many reports for mercury removal using Cu-BTC.

In this study, Cu-BTC was prepared and used for elemental mercury removal from the sintering gas. The mercury removal performance was investigated under different work conditions, and the influence of temperature, O_2 concentration, HCl concentration and other gas components (including SO_2, NO and H_2O) was examine. Besides, the mercury removal mechanism was also discussed according to the results of mercury removal performance and physiochemical characterization.

2. Experimental

2.1. Preparation of catalysts

Cu-BTC was prepared by hydrothermal method. 2.078 g (8.6 mmol) $Cu(NO_3)_2{\cdot}3H_2O$ was dissolved in 20 mL deionized water, then 1.056 g (5 mmol) 1,3,5-Benzenetri-carboxylic acid (H_3BTC) dissolved in 20 mL N,N-dimethylformamide (DMF) and 20 mL absolute ethanol was added into the solution. After 30 min of stirring, the mixed solution was transferred to a Teflon-lined autoclave and heated at 110 °C for 18 h. The recovered blue crystals were washed with DMF and absolute ethanol for several times, and dried in vacuum at 110 °C overnight.

2.2. Material characterization

The morphology and structure of Cu-BTC were observed by JEM-2010HT transmission electron microscope (TEM), and samples were dispersed in ethanol with strong sonication before the analysis. Thermo gravimetric analysis (TGA) was conducted with Mettler Toledo thermo gravimetric analyzer to see the stability of Cu-BTC, and the ramp rate for the TGA was 10 °C/min from 30 to 700 °C. The Brunauer–Emmett–Teller (BET) surface area was measured using Nova-2200e adsorption system (Quantachrome Nova 2200e), and the pore volume was calculated by Barrett–Joyner–Halenda (BJH) method. X-ray diffraction (XRD) data was recorded by SHIMADZU XRD-6100 diffractometer with Cu Kα radiation (40 kV, 20 mA), and the scanning range was from 5° to 30° with a scanning rate of 10°/min. The X-ray photoelectron spectroscopy (XPS) was measured by Kratos Axis Ultra-DLD spectrometer with Al Kα radiation source, and The C 1s line at 284.8 eV was taken as a reference for binding energy calibration.

2.3. Mercury removal studies

The experiment system is shown as Fig. 1. The whole system

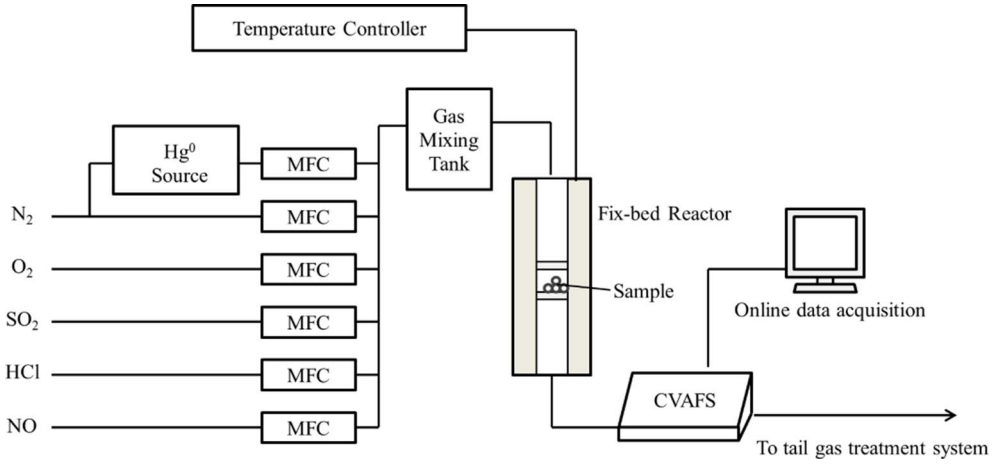

Fig. 1. The experiment system for mercury removal studies.

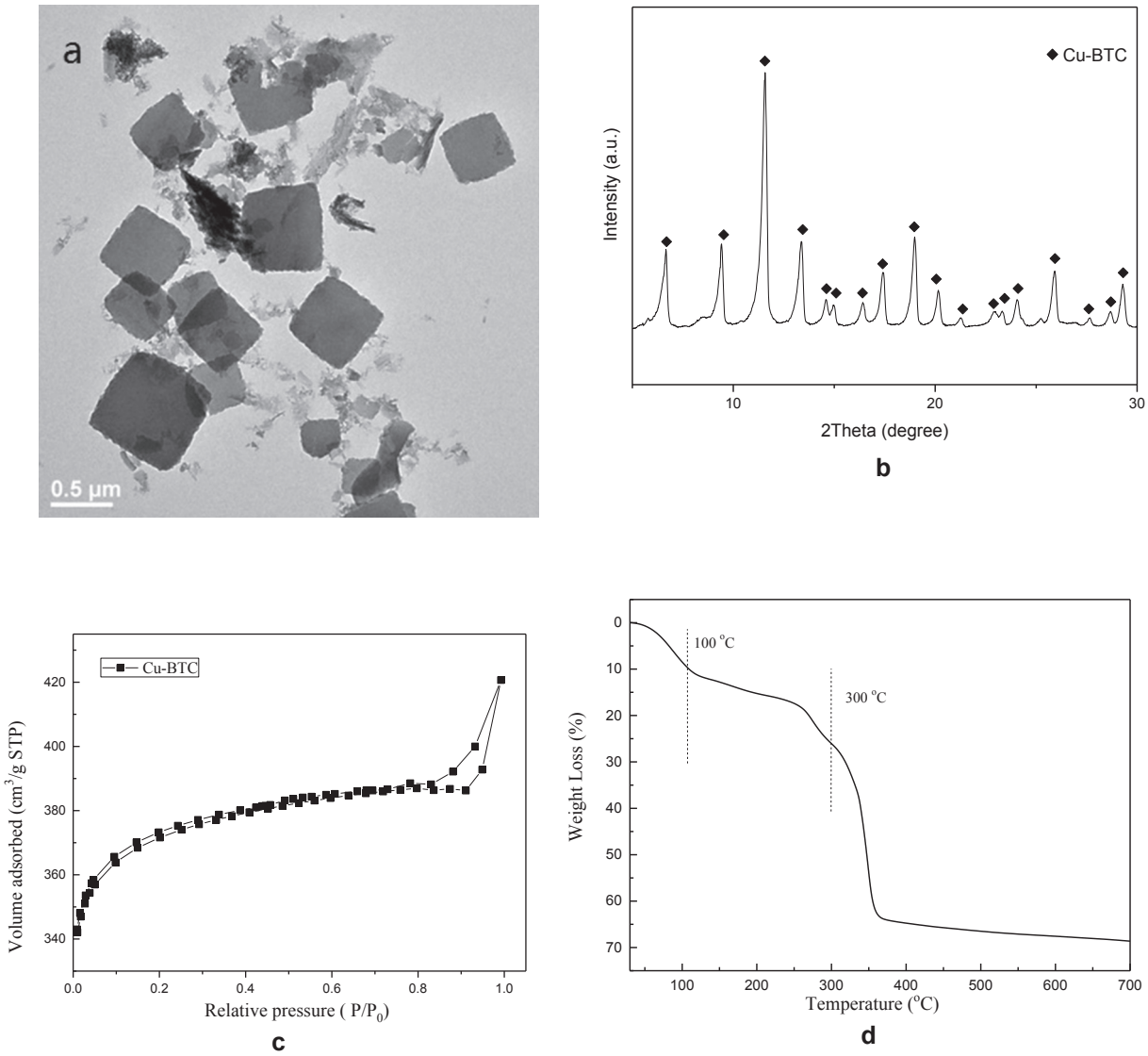

Fig. 2. The physiochemical characterization results of Cu-BTC: (a) TEM images of Cu-BTC, (b) XRD patterns of Cu-BTC, (c) sorption isotherms of N_2 on Cu-BTC, and (d) TGA curve of Cu-BTC.

Table 1
The BET surface area and the pore volume of Cu-BTC and other adsorbents.

Adsorbents	$S_{BET}/(m^2 \cdot g^{-1})$	Pore Volume/$(cc \cdot g^{-1})$
Cu-BTC	1189.662	0.53
Activated carbon [39]	860	0.55
Zeolite 2,3 [40–42]	355–655	0.16–0.3

consists of a simulated gas preparation system, a fix-bed reactor with temperature controller, a cold vapor atomic fluorescence spectrometry (CVAFS) and an online data acquisition system. The composition of simulated gas can be controlled by the mass flow controller (MFC), and each constituent of the gas was thoroughly mixed with others in a mixing tank. The flow rate of the gas was 350 mL/min, corresponding with a space velocity (SV) of $3.64 \times 10^5\ h^{-1}$. An Hg^0 permeation tube was used to generate Hg^0 vapor carried by pure N_2, which was then introduced to the inlet of the gas mixer. The inlet concentration of Hg^0 was around 200 μg/m^3. CVAFS analyzer was employed as an online continuous detector that could only detect Hg^0. The concentration of Hg^0 was measured using Lumex RA 915+. In each test, the simulated gas firstly passed through the bypass and the baseline of Hg^0 was determined by CVAFS. Then the gas was diverted to the fix-bed reactor containing 20 mg of sample. The mercury removal performance was investigated under different temperature (25–250 C), O_2 concentration (2–10%), and HCl concentration (5–15 ppm). The influence of SO_2 (100 ppm), NO (100 ppm) and H_2O (10%) was also studied. The Hg^0 removal efficiency can be calculated using the follow formula: $E = \frac{Hg^0_{in} - Hg^0_{out}}{Hg^0_{in}}$ where E is the mercury removal efficiency, Hg^0_{in} and Hg^0_{out} are respectively the inlet and outlet concentration of Hg^0.

3. Results and discussion

3.1. The physiochemical characterization of Cu-BTC

To obtain the microscopic morphologies and structural information, transmission electron microscopy (TEM) analysis of Cu-BTC was performed, as shown in Fig. 2(a). It can be found that Cu-BTC exhibits octahedral-shaped crystals with good dispersivity. Besides, the particle size was nearly 400–600 nm. Some differences from the reported features of Cu-BTC may be caused by the difference of reaction temperature and reaction pressure [35].

Fig. 2(b) shows the XRD pattern of Cu-BTC, which is consistent with

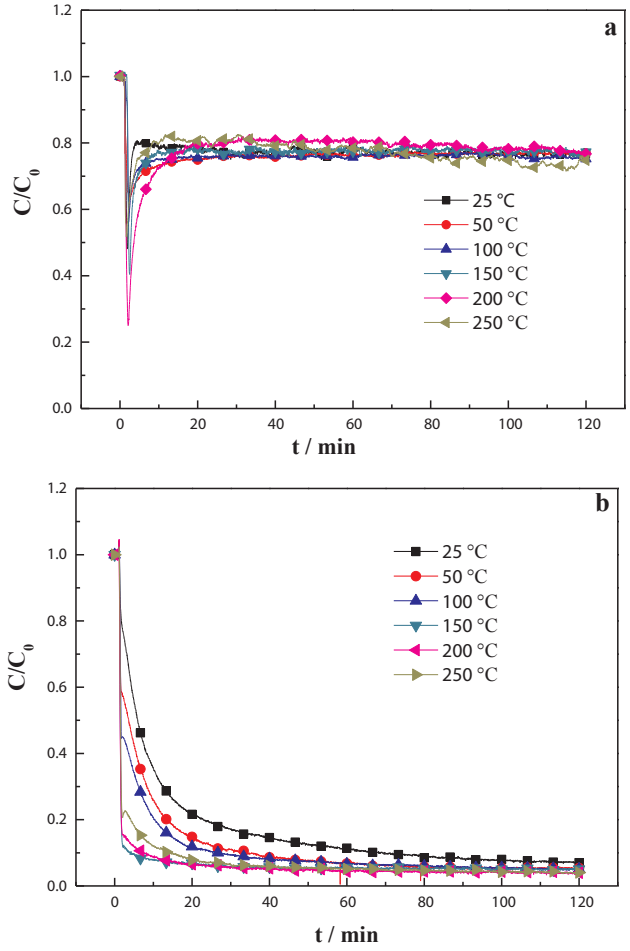

Fig. 3. The Hg^0 removal performance at different temperatures: (a) without HCl; (b) with the existence of 15 ppm HCl in different temperature.

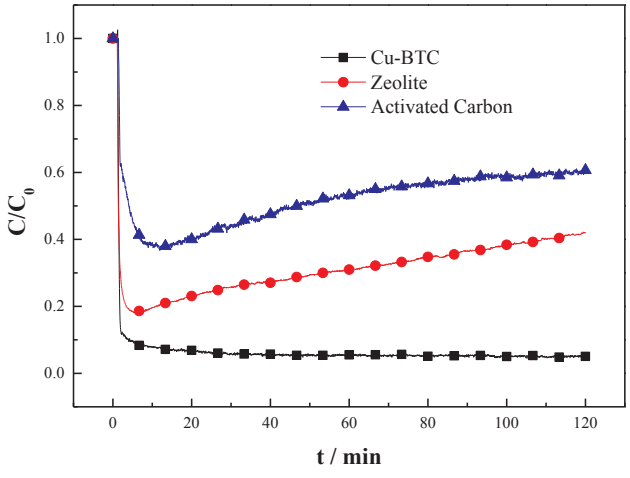

Fig. 4. The comparison between the Hg^0 removal performance of Cu-BTC and that of zeolite and activated carbon.

the previous report [36], and the peaks at around 2θ = 14.5° corresponds to the characteristic of Cu-BTC [37]. It indicates that Cu-BTC is successfully prepared.

The N_2 sorption-desorption isotherm is shown in Fig. 2(c), which was assigned to type IV according to the IUPAC classification and exhibited a type H1 hysteresis at high relative pressure, which means Cu-BTC is microporous solid with narrow slit-like pores [38]. As seen in Table 1, the BET surface area and the pore volume of Cu-BTC were

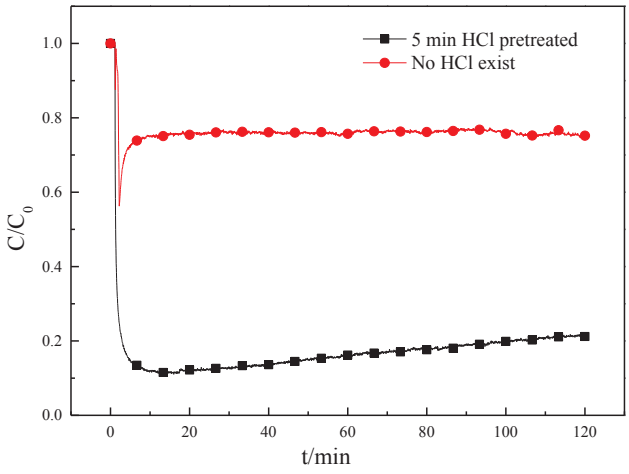

Fig. 5. The Hg^0 removal performance after 5 min's adsorption of HCl.

Table 2
The Hg adsorption capability of Cu-BTC in different conditions.

Conditions	Hg adsorption capability /(mg·g^{-1})	HCl content/ (mg·g^{-1})
5 min HCl pretreated	1.7	2.1
No HCl exist	0.084	——

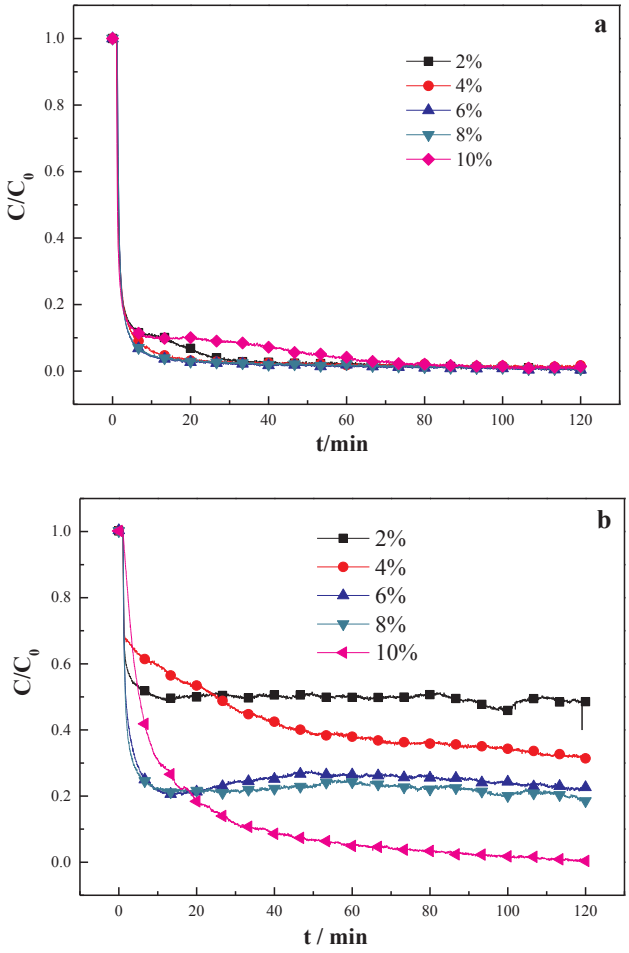

Fig. 6. The influence of O_2 concentration with (a) 15 ppm HCl and (b)5 ppm HCl.

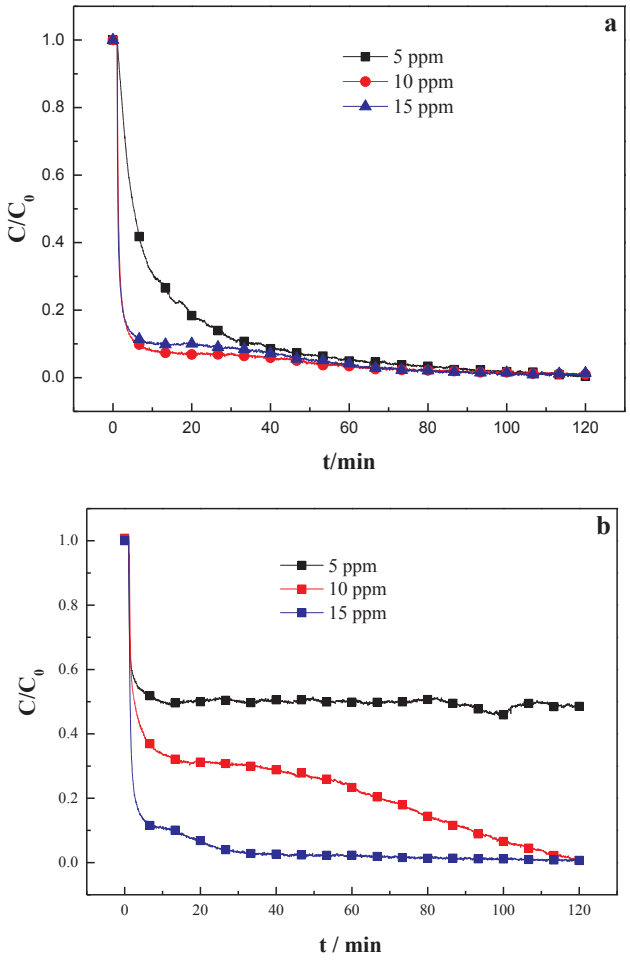

Fig. 7. The influence of HCl concentration with (a) 10% O_2 and (b) 2% O_2.

respectively determined to be 1189.662 m^2/g and 0.53 cc/g, which were larger than that of the conventional adsorbents. A large specific surface area is advantageous for mercury removal.

The result of TGA is illustrated in Fig. 2(d). There were three weight loss change trend. The weights loss of Cu-BTC below 100 °C might be attributed to the loss of physically adsorbed water, guest water and solvent molecules. And the weights loss between 100 °C and 300 °C was assigned to the organic residues. The weights loss changed rapidly above 300 °C, which demonstrating the structure collapse of catalysts. The results above shows that Cu-BTC is stable up to a temperature of about 300 °C. Therefore, the suitable operational temperature of Cu-BTC should be under 300 °C. Since the temperature of sintering gas is 120–180 °C [17], Cu-BTC is thermal stable in sintering gas and can be used for removing Hg^0 at this condition.

3.2. Hg^0 removal performance

The Hg^0 removal performance was investigated at different temperatures with the gas component of Hg^0 + 10% O_2, shown in Fig. 3(a). It can be seen that the impact of temperature on Hg^0 removal performance is not significant, and the Hg^0 removal efficiency was around 24% at various temperatures. In this gas condition, the mercury removal ability of Cu-BTC was not very good.

However, when 15 ppm HCl was added, the Hg^0 removal efficiency was significantly increased, shown in Fig. 3(b). When temperature increased from 25 °C to 150 °C, the Hg^0 removal efficiency slightly increased from 93% to 96%,and then maintained approximately 96% in the temperature range of 150–250 °C. In all, from 25 to 250 °C, Cu-BTC showed excellent Hg^0 removal capacity in the present of HCl. Since HCl exists in sintering gas, Cu-BTC is well suited for Hg^0 removal.

The Hg^0 removal efficiencies of Cu-BTC, zeolite and activated carbon are shown in Fig. 4. The experiment was conducted at a typical temperature of sintering gas (150 °C) with the gas component of Hg^0 + 10% O_2 + 15 ppm HCl. Obviously, the Hg^0 removal performance of Cu-BTC was best.

To explore the effect of HCl, another Hg^0 removal experiment was conducted: the sample was pretreated with 15 ppm HCl for 5 min and then purged with N_2 for 30 min. Next, Hg^0 with 10% O_2 was passed through the sample. The temperature of the experiment was kept at 150 °C. Finally, after saturate adsorption, the mercury content was determined by mercury analyzer (Lumex RA 915+, Lumex, Russia) to obtain the mercury adsorption capability. Besides, the mercury adsorption capability in the condition of without HCl was also measured. Fig. 5 shows the Hg° Concentration changes of HCl-pretreated Cu-BTC. As seen in Fig. 5, the sample still had high Hg^0 removal efficiency without HCl. And the mercury adsorption capability was up to 1.7 mg/g, while without HCl, the mercury adsorption capability was only 84 μg/g. (Table 2) Moreover, after 5 min's HCl adsorption and 30 min's N_2 purge, the HCl content of the sample was determined by a microcoulomb analyzer (WK-2D, Jiangfen, China), and 2.1 mg/g HCl was found on the sample. The above result illustrated that Cu-BTC has strong adsorption capacity for HCl. That may be the main reason why Cu-BTC showed better Hg^0 removal performance than zeolite and activated carbon. After HCl adsorption, the adsorption capacity for mercury can be substantially improved. Furthermore, since the sample was purged by nitrogen, HCl may be chemically adsorbed by the material or enter into the channels, instead of physically adsorption on the surface.

To further understand the Hg removal performance in the presence of HCl, the influence of O_2 and HCl concentration was studied, shown in Figs. 6and 7. The temperature was 150 °C. Fig. 6(a) shows that O_2 concentration had little influence on the Hg^0 removal efficiency when the HCl concentration was 15 ppm. Similarly, in the condition of 10% O_2, the effect of HCl concentration was less (Fig. 7(a)). However, for HCl and O_2, if one of them was at low concentration, the influence of the other would be significant (Figs. 6(b) and 7(b)). Higher HCl concentration caused higher Hg^0 removal efficiency with only 2% O_2 in the gas. And in the condition of 5 ppm HCl, higher O_2 concentration resulted in better Hg^0 removal performance. The above results indicated that both HCl and O_2 played an important role in the removal of Hg^0.

Moreover, the influence of SO_2 (100 ppm), NO (100 ppm) and H_2O were studied in typical sintering gas conditions (150 °C, 15 ppm HCl, 10% O_2), shown in Fig. 8. When SO_2 was introduced, the Hg^0 removal efficiency slightly decreased (Fig. 8(a)), and when NO was in the inlet gas, no significant change on Hg^0 removal efficiency was found (Fig. 8(b)). Also, the Hg^0 removal efficiency did not change significantly when H_2O was in the inlet gas (Fig. 8(c)). This may be because the Hg^0 removal efficiency is already high due to the high concentration of HCl and O_2 that the influence of SO_2, NO and H_2O was small. Therefore, another experiment was conducted when HCl and O_2 were at low concentration (5 ppm HCl, 2% O_2). As shown in Fig. 8(e), when SO_2 was passed, the Hg^0 removal efficiency decreased more significantly, and an increase of the Hg^0 removal efficiency was observed when NO was in the inlet gas (Fig. 8(f)). When there was H_2O in the gas, no significant change on Hg^0 removal efficiency was found (Fig. 8(g)). Furthermore, the influence of coexistence of HCl, SO_2, NO and H_2O on Hg^0 removal was investigated. In typical sintering gas conditions (150 °C, 15 ppm HCl, 10% O_2), the Hg^0 removal rate was slightly decreased (Fig. 8(d)). Similar result was also found when HCl and O_2 were at low concentration (5 ppm HCl, 2% O_2) (Fig. 8(h)). In conclusion, SO_2 has inhibition effect on the removal of Hg^0, while NO can promote the Hg^0 removal. As for H_2O, it has nearly no effects on mercury removal. When HCl and O_2 are at high concentration, the influence of SO_2, NO and H_2O are not significant. And the influence on Hg^0 removal under the coexistence of HCl, SO_2, NO and H_2O is also not significant. That means in typical sintering gas condition, Cu-BTC can still have high Hg^0

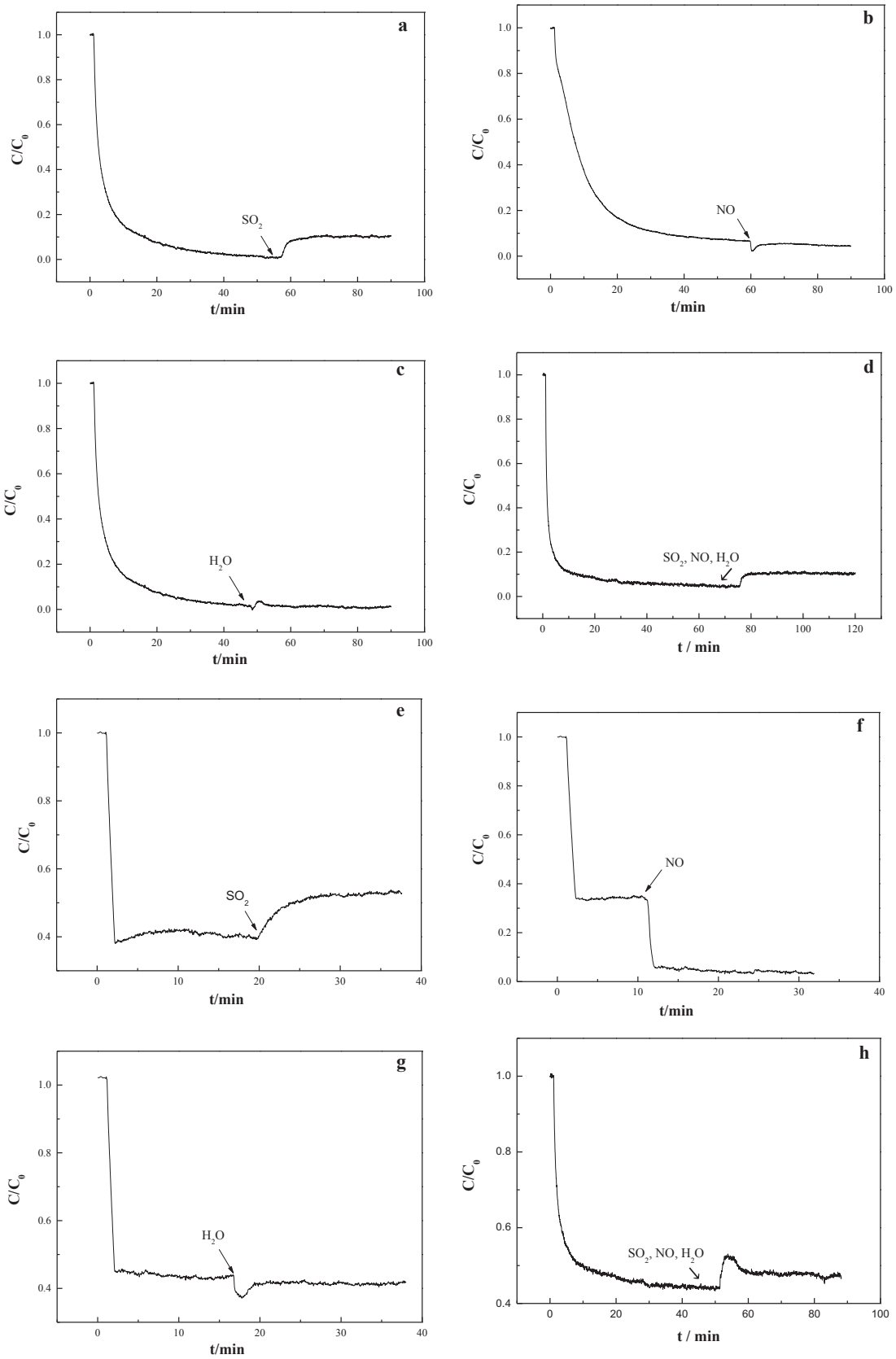

Fig. 8. The influence of gas composition: (a) SO_2, (b) NO, (c) H_2O and (d) coexistence of HCl, SO_2, NO and H_2O in the condition of 15 ppm HCl and 10% O_2; (e) SO_2, (f) NO, (g) H_2O and (h) coexistence of HCl, SO_2, NO and H_2O in the condition of 5 ppm HCl and 2% O_2.

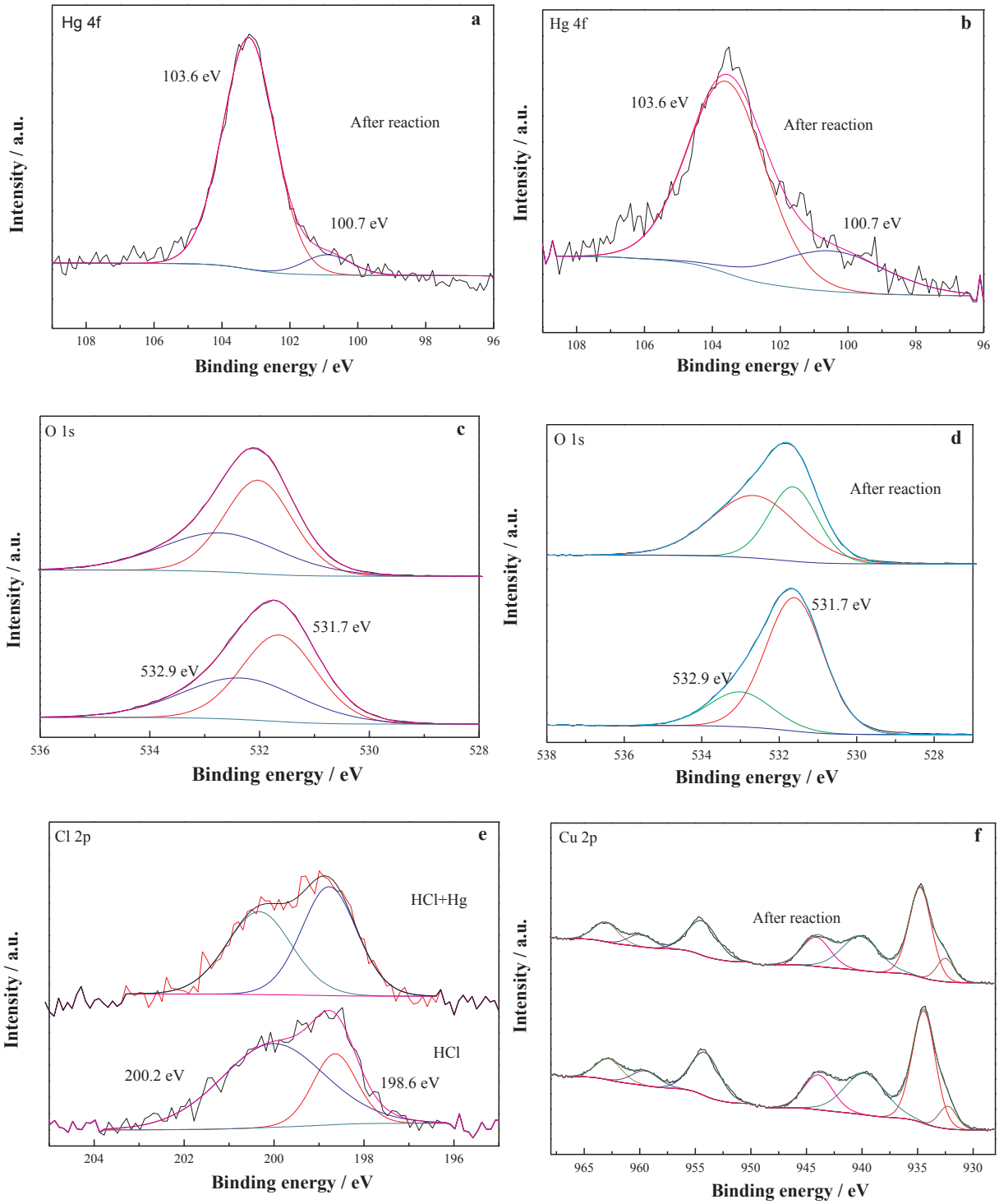

Fig. 9. XPS spectra of Cu-BTC over the spectral regions: (a) Hg 4f after reaction with Hg + O_2, (b) Hg 4f after reaction with Hg + O_2 + HCl, (c) O 1s after reaction with Hg + O_2, (d) O 1s after reaction with Hg + O_2 + HCl, (d) Cl 2p, (e) Cu 2p after reaction with Hg + O_2, and (f) Cu 2p after reaction with Hg + O_2 + HCl.

removal efficiency with the existence of other gas.

3.3. Hg^0 removal mechanism

XPS spectra was also measured to explore the Hg^0 removal mechanism. Fig. 8 shows the XPS spectra of Cu-BTC over the spectral regions of Hg 4f, O 1s, Cl 2p and Cu 2p.

Fig. 9(a) and (b) recorded the Hg 4f XPS spectrum. The peak at 100.7 eV was assigned to Hg^{2+}, and the peak intensity was weaker than that when HCl existed. Some Hg^0 might be oxidized by active oxygen to HgO when no HCl existed. After adding HCl, the characteristic peak intensity increased obviously, implied that Hg^0 may be oxidized by active Cl to $HgCl_2$ with the existence of HCl, besides, the generated HgO also react with HCl to produced $HgCl_2$. As for the peak at 103.6 eV, it might be the peak of Si from Silica wool, which was used for supporting the sample.

The O 1s spectrum is shown in Fig. 9(c) and (d). The peak at 531.4 eV was attributed to the chemisorbed oxygen. And the peak at about 533 eV was assigned to the oxygen components on the carboxylate groups (O—C═O) due to the residues of organic ligand. After

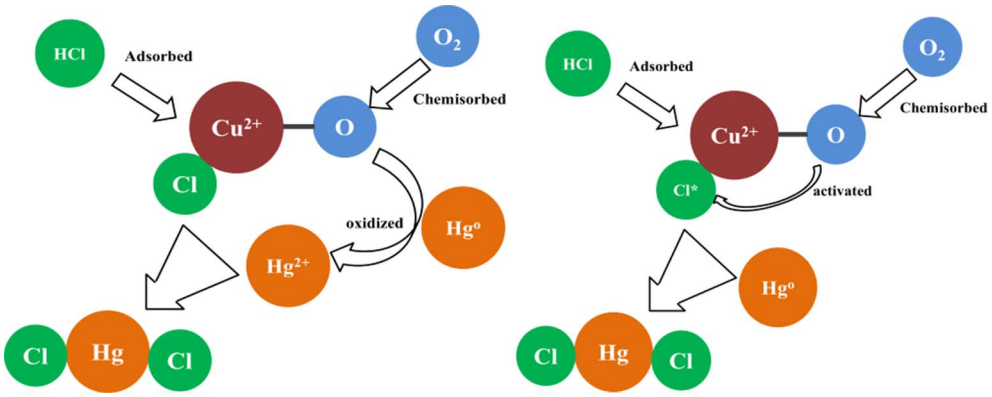

Fig. 10. The reaction process for the Hg^0 removal over Cu-BTC.

reaction with Hg + O_2 + HCl, the amount of chemisorbed oxygen (531.7 eV) decreased (Fig. 9(d)), while the O 1s spectrum did not change significantly after reaction with Hg + O_2 (Fig. 9(c)). It suggests that chemisorbed oxygen participated in the oxidation of Hg^0 with the existence of HCl.

The Cl 2p spectrum is shown in Fig. 9(e). The peak at 198.6 eV and 200.2 eV were respectively attributed to ionic and covalent chlorine species, respectively [43]. The ionic species may be produced $HgCl_2$ by the reaction of Hg^0 and active Cl, or the intermediate of CuCl or $CuCl_2$ by the reaction of Cu open metal site and HCl. Besides, the covalent chlorine species may be the adsorbed HCl. After reaction with Hg^0, the ionic species significantly increased, which means $HgCl_2$ was generated during the reaction.

The Cu 2p spectrum is shown in Fig. 9(f) and (g). After reaction without HCl, no significant change in valence state of Cu was found. When HCl existed in the gas, the result was similar. That means without HCl, the role of Cu may be not significant, and with the existence of HCl, Cu plays a catalytic role in mercury removal. Besides, Cu in Cu-BTC is the unsaturated metal site, which may be helpful for Cu to play the catalytic role better.

Based on the above results, the Hg^0 removal mechanism can be speculated as follows, shown in Fig. 10: when there is no HCl in the gas, Hg^0 is removed mainly by active oxygen to generate HgO; with the existence of HCl, Cu-BTC can absorb the HCl to form the intermediate of CuCl or $CuCl_2$, then Hg^0 is captured and oxidized to Hg^{2+} by the chemisorbed O_2, and finally reacts with $CuCl/CuCl_2$ to produced $HgCl_2$. Besides, active Cl might be generated by active oxygen and then oxidized Hg^0 to $HgCl_2$. Cu plays a catalytic role during the reaction.

4. Conclusions

By a facile method, Cu-BTC was successfully synthesized as a novel material for removal of Hg^0. Cu-BTC has good physical and chemical properties that suitable for sintering gas. Although the Hg^0 removal ability of Cu-BTC was limited when there were only Hg, N_2 and O_2 in the gas, it can be extremely improved by HCl. HCl and O_2 influenced the Hg^0 removal efficiency when they were at low concentration. Without HCl, Hg^0 is removed mainly by active oxygen. In the present of HCl, the Hg^0 removal mechanism can be described as: HCl is strongly absorbed by Cu-BTC to form the intermediate of CuCl or $CuCl_2$, then Hg^0 is captured and oxidized to Hg^{2+} by the chemisorbed O_2 and finally reacted with $CuCl/CuCl_2$ to produced $HgCl_2$; besides, active Cl might be generated by active oxygen and then oxidized Hg^0 to $HgCl_2$; Cu plays a catalytic role during the reaction. Furthermore, SO_2 has inhibition effect on the removal of Hg^0, while NO can promote the Hg^0 removal. As for H_2O, it has nearly no effects on mercury removal. In a typical sintering gas condition where HCl and O_2 concentration were high, the influence of SO_2, NO and H_2O are not pronounced. The above results show that Cu-BTC can be a promising sorbent for capturing Hg^0 from sintering gas.

Acknowledgements

This study was supported by the National Key Research and Development Program of China (No. 2017YFC0210500) and the National Natural Science Foundation of China (No. 21677096) and (No. 21607102), and China's Post-doctoral Science Fun (No. 2015M581626).

References

[1] Abbas T, Nazir S, Øvergård KI, Manca D, Mutalib A, Khan E. Hazards of mercury – safety perspectives and measures. Chem Eng Trans 2015;43:2143–8.
[2] Weiss-Penzias PS, Gay DA, Brigham ME, Parsons MT, Gustin MS, Ter SA. Trends in mercury wet deposition and mercury air concentrations across the U.S. and Canada. Sci Total Environ 2016;568:546–56.
[3] Selin NE. Global biogeochemical cycling of mercury: a review. Annu Rev Environ Resour 2010;34(1):43–63.
[4] Gilmour CC, Podar M, Bullock AL, Graham AM, Brown SD, Somenahally AC, et al. Mercury methylation by novel microorganisms from new environments. Environ Sci Technol 2013;47(20):11810.
[5] Mcnutt M. Mercury and health. Science 2013;341(6153):1430.
[6] Sundseth K, Pacyna JM, Pacyna EG, Pirrone N, Thorne RJ. Global sources and pathways of mercury in the context of human health. Int J Environ Res Public Health 2017;14(1):105.
[7] Assessment UGM. Sources, emissions, releases and environmental transport; 2013.
[8] Xu W, Shao M, Yang Y, Liu R, Wu Y, Zhu T. Mercury emission from sintering process in the iron and steel industry of China. Fuel Process Technol 2017;159:340–4.
[9] Feng X, Streets D, Hao J, Wu Y, Li G. Mercury emissions from industrial sources in China. US: Springer; 2009. p. 67–79.
[10] Wong CSC, Duzgoren-Aydin NS, Aydin A, Ming HW. Sources and trends of environmental mercury emissions in Asia. Sci Total Environ 2006;368:649–62.
[11] Wang S, Luo K. Atmospheric emission of mercury due to combustion of steam coal and domestic coal in China. Atmos Environ 2017;162:45–54.
[12] Zhang L, Wang S, Wang L, Wu Y, Duan L, Wu Q, et al. Updated emission inventories for speciated atmospheric mercury from anthropogenic sources in China. Environ Sci Technol 2015;49(5):3185–94.
[13] Hua S, Tian H, Wang K, Zhu C, Gao J, Ma Y, et al. Atmospheric emission inventory of hazardous air pollutants from China's cement plants: temporal trends, spatial variation characteristics and scenario projections. Atmos Environ 2016;128:1–9.
[14] Wang F, Wang S, Lei Z, Hai Y, Wei G, Wu Q, et al. Mercury mass flow in iron and steel production process and its implications for mercury emission control. J Environ Sci 2016;43:293–301.
[15] Srivastava RK, Hutson N, Martin B, Princiotta F, Staudt J. Control of mercury emissions from coal-fired electric utility boilers. Environ Sci Technol 2006;40:1385–93.
[16] Liu R, Xu W, Tong L, Zhu T. Role of NO in Hg oxidation over a commercial selective catalytic reduction catalyst V2O5–WO3/TiO2. J Environ Sci 2015;38(12):126–32.
[17] Zhou JA, Zhong SJ, Dang JX, Li X. Experimental investigation of sintering flue gas desulfurization with steel slag using dry CFB method. Appl Mech Mater 2011;71–78:2547–50.
[18] Xu H, Zan Q, Zong C, Quan F, Jian M, Yan N. Catalytic oxidation and adsorption of Hg^0 over low-temperature NH_3-SCR $LaMnO_3$ perovskite oxide from flue gas. Appl Catal B 2016;186:30–40.
[19] Abbas T, Gonfa G, Lethesh KC, Mutalib MIA, Abai MB, Cheun KY, et al. Mercury capture from natural gas by carbon supported ionic liquids: Synthesis, evaluation and molecular mechanism. Fuel 2016;177(August):296–303.
[20] Abai M, Atkins MP, Hassan A, Holbrey JD, Kuah Y, Nockemann P, et al. An ionic liquid process for mercury removal from natural gas. Dalton Trans 2015;44(18):8617–24.
[21] Zhang W, Lu G, Cui C, Liu Y, Li S, Yan W, et al. A family of metal-organic frameworks exhibiting size-selective catalysis with encapsulated noble-metal nanoparticles. Adv Mater 2014;26:4056–60.
[22] Dong W, Feng C, Zhang L, Shang N, Gao S, Wang C, et al. Pd@UiO-66: an efficient

catalyst for Suzuki-Miyaura coupling reaction at mild condition. Catal Lett 2016;146:117–25.
[23] Srinivas G, Krungleviciute V, Guo ZX, Yildirim T. Exceptional CO_2 capture in a hierarchically porous carbon with simultaneous high surface area and pore volume. Energy Environ Sci 2014;7:335–42.
[24] Ren J, Langmi HW, North BC, Mathe M, Bessarabov D. Modulated synthesis of zirconium-metal organic framework (Zr-MOF) for hydrogen storage applications. Int J Hydrogen Energy 2014;39:890–5.
[25] Wu H, Chua YS, Krungleviciute V, Tyagi M, Chen P, Yildirim T, et al. Unusual and highly tunable missing-linker defects in zirconium metal-organic framework UiO-66 and their important effects on gas adsorption. J Am Chem Soc 2013;135:10525.
[26] Horcajada P, Gref R, Baati T, Allan PK, Maurin G, Couvreur P, et al. Metal-organic frameworks in biomedicine. Chem Rev 2012;112:1232–68.
[27] Zubair H, Sung Hwa J. Removal of hazardous organics from water using metal-organic frameworks (MOFs): plausible mechanisms for selective adsorptions. J Hazard Mater 2015;283:329–39.
[28] Wang CC, Li JR, Lv XL, Zhang YQ, Guo G. Photocatalytic organic pollutants degradation in metal–organic frameworks. Energy Environ Sci 2014;7:2831–67.
[29] Barea E, Montoro C, Navarro JAR. Toxic gas removal - metal-organic frameworks for the capture and degradation of toxic gases and vapours. Chem Soc Rev 2014;43(16):5419–30.
[30] Ke F, Qiu LG, Yuan YP, Peng FM, Jiang X, Xie AJ, et al. Thiol-functionalization of metal-organic framework by a facile coordination-based postsynthetic strategy and enhanced removal of Hg^{2+} from water. J Hazard Mater 2011;196:36–43.
[31] Chui SS, Lo SM, Charmant JP, Orpen AG, Williams ID. A chemically functionalizable nanoporous material. Science 1999;283:1148.
[32] Pérezmayoral E, Musilová Z, Gil B, Marszalek B, Položij M, Nachtigall P. Synthesis of quinolines via Friedlander reaction catalyzed by CuBTC metal-organic-framework. Dalton Trans 2012;41:4036–44.
[33] Položij M, Rubeš M, Čejka J, Nachtigall P. Catalysis by dynamically formed defects in a metal-organic framework structure: knoevenagel reaction catalyzed by copper benzene-1,3,5-tricarboxylate. ChemCatChem 2015;6:2821–4.
[34] Assche TRCV, Duerinck T, Sevillano JJG, Calero S, Baron GV, Denayer JFM. High adsorption capacities and two-step adsorption of polar adsorbates on copper- benzene-1,3,5-tricarboxylate metal-organic framework. J Phys Chem C 2013;117:18100–11.
[35] Wang QM, Shen D, Bülow M, Lau ML, Deng S, Fitch FR, et al. Metallo-organic molecular sieve for gas separation and purification. Microporous Mesoporous Mater 2002;55:217–30.
[36] Sun B, Kayal S, Chakraborty A. Study of HKUST (Copper benzene-1,3,5-tricarboxylate, Cu-BTC MOF)-1 metal organic frameworks for CH_4 adsorption: An experimental Investigation with GCMC (grand canonical Monte-carlo) simulation. Energy 2014;76:419–27.
[37] Schlichte K, Kratzke T, Kaskel S. Improved synthesis, thermal stability and catalytic properties of the metal-organic framework compound CU3(BTC)(2). Microporous Mesoporous Mater 2004;73:81–8.
[38] Sing KSW. Reporting physisorption data for gas/solid systems with special reference to the determination of surface area and porosity (Recommendations 1984). Pure Appl Chem 1985;57:603–19.
[39] Herawan SG, Hadi MS, Ayob MR, Putra A. Characterization of activated carbons from oil-palm shell by CO_2 activation with no holding carbonization temperature. Sci World J 2013;2013:624865.
[40] Khanday WA, Majid SA, Shekar SC, Tomar R. Synthesis and characterization of various zeolites and study of dynamic adsorption of dimethyl methyl phosphate over them. Mater Res Bull 2013;48:4679–86.
[41] Chen SJ, Zhu M, Fu Y, Huang YX, Tao ZC, Li WL. Using 13X, LiX, and LiPdAgX zeolites for CO_2 capture from post-combustion flue gas. Appl Energy 2017;191:87–98.
[42] Chung KH. High-pressure hydrogen storage on microporous zeolites with varying pore properties. Energy 2010;35:2235–41.
[43] Cao Y, Yu Y, Zhang P, Zhang L, He T, Cao Y. An enhanced visible-light photocatalytic activity of TiO_2 by nitrogen and nickel–chlorine modification. Sep Purif Technol 2013;104:256–62.